AMERICAN SOCIETY FOR MICROBIOLOGY | Journal of Virology®

VIRUS-CELL INTERACTIONS

Variations in Cell Surface ACE2 Levels Alter Direct Binding of SARS-CoV-2 Spike Protein and Viral Infectivity: Implications for Measuring Spike Protein Interactions with Animal ACE2 Orthologs

Soheila Kazemi,[a] Alberto Domingo López-Muñoz,[b] Jaroslav Hollý,[b] Ling Jin,[a] Jonathan W. Yewdell,[b] Brian P. Dolan[a]

[a]Department of Biomedical Sciences, Carlson College of Veterinary Medicine, Oregon State University, Corvallis, Oregon, USA
[b]Laboratory of Viral Diseases, Cell Biology Section, National Institute of Allergy and Infectious Diseases, National Institutes of Health, Bethesda, Maryland, USA

ABSTRACT Severe acute respiratory syndrome coronavirus 2 (SARS-CoV-2) is the causative agent of coronavirus disease 2019 (COVID-19), the most severe pandemic in a century. The virus gains access to host cells when the viral spike protein (S-protein) binds to the host cell surface receptor angiotensin-converting enzyme 2 (ACE2). Studies have attempted to understand SARS-CoV-2 S-protein interactions with vertebrate orthologs of ACE2 by expressing ACE2 orthologs in mammalian cells and measuring viral infection or S-protein binding. Often, these cells only transiently express ACE2 proteins, and the levels of ACE2 at the cell surface are not quantified. Here, we describe a cell-based assay that uses stably transfected cells expressing ACE2 proteins in a bicistronic vector with an easy-to-quantify reporter protein, Thy1.1. We found that both the binding of the S-protein receptor-binding domain (RBD) and infection with a SARS-CoV-2 pseudovirus are proportional to the amount of human ACE2 expressed at the cell surface, which can be inferred by quantifying the level of Thy1.1. We also compared different ACE2 orthologs, which were expressed in stably transfected cells expressing equivalent levels of Thy1.1. When ranked for either viral infectivity or RBD binding, mouse ACE2 had a weak to undetectable affinity for S-protein, while human ACE2 had the highest level detected, and feline ACE2 had an intermediate phenotype. The generation of stably transfected cells whose ACE2 level can be normalized for cross-ortholog comparisons allows us to create a reusable cellular library useful for measuring emerging SARS-CoV-2 variants' abilities to potentially infect different animals.

IMPORTANCE SARS-CoV-2 is a zoonotic virus responsible for the worst global pandemic in a century. An understanding of how the virus can infect other vertebrate species is important for controlling viral spread and understanding the natural history of the virus. Here, we describe a method to generate cells stably expressing different orthologs of ACE2, the receptor for SARS-CoV-2, on the surface of a human cell line. We find that both the binding of the viral spike protein receptor-binding domain (RBD) and infection of cells with a SARS-CoV-2 pseudovirus are proportional to the ACE2 levels at the cell surface. This method will allow the creation of a library of stably transfected cells expressing similar levels of different vertebrate ACE2 orthologs, which can be used repeatedly for identifying vertebrate species that may be susceptible to infection with SARS-CoV-2 and its many variants.

KEYWORDS ACE2 orthologs, SARS-CoV-2

The worldwide severe acute respiratory syndrome coronavirus 2 (SARS-CoV-2) pandemic gave rise to an urgent need for accurate diagnosis, effective treatment, and vaccine development. Rapid progress has been made in elucidating the steps of virus entry into cells. It is well established that angiotensin-converting enzyme 2 (ACE2) serves as the

Editor Kanta Subbarao, The Peter Doherty Institute for Infection and Immunity

Address correspondence to Brian P. Dolan, Brian.Dolan@oregonstate.edu.

The authors declare no conflict of interest.

Received 8 February 2022
Accepted 4 August 2022
Published 24 August 2022

cell surface receptor for both SARS-CoV-1 and SARS-CoV-2, although other molecules no doubt play an important role in viral infectivity (1–5). Due to the zoonotic nature of SARS-CoV-2 infection, there have been numerous studies attempting to understand how different vertebrate ACE2 orthologs can interact with the spike protein (S-protein) of SARS-CoV-2 (6–9). This knowledge is necessary not only to understand the natural history of the virus but also to identify species that may be more susceptible to infection. Even though ACE2 is a well-conserved protein across the vertebrate clade, human polymorphisms have been documented (10), and ACE2 orthologs from different animals have unique amino acid sequences, which potentially alter the ability of a particular S-protein to bind to specific cells (11, 12). The difference in ACE2 orthologs is thought to be a potential mechanism by which certain species appear to be protected from infection or how other species can act as an intermediate when SARS-like coronaviruses transition between host species (13, 14).

Since the beginning of the current global pandemic, there have been multiple studies attempting to determine which ACE2 orthologs serve as receptors for S-protein. These studies include (i) *in silico* models that predict which orthologs would be likely to bind S-protein based upon amino acid residues known to interact with S-protein (4, 9, 15–25), (ii) *in vitro* cell-based studies where viral infectivity in cells from different animals or cell lines genetically modified to express different ACE2 orthologs is examined for interactions with S-protein (or its receptor-binding domain [RBD]) or infection with the virus or S-protein-expressing pseudovirus (2, 6, 11, 26–30), and (iii) biochemical studies measuring the binding of S-protein with different ACE2 proteins (31, 32). There are advantages and drawbacks to each approach. *In silico* modeling enables the rapid comparison of multiple orthologs but is limited to publicly available genetic data, and predictions need to be validated experimentally. The biochemical measurement of the SARS-CoV-2 S-protein–ACE2 association provides an accurate measurement of the binding affinity between the two proteins but requires the production and purification of each ACE2 ortholog and the SARS-CoV-2 S-protein or RBD and does not necessarily reflect associations in the context of physiological virus-cell interactions. Cell infectivity or binding of soluble SARS-CoV-2 S-protein can provide information about which ACE2 orthologs can successfully interact with S-protein at the cell surface. However, it requires genetically modifying cells by plasmid transfection or lentiviral transduction with each ACE2 ortholog, and controlling for the level of ACE2 at the cell surface is difficult.

In vitro infection studies with multiple different types of viruses have demonstrated that the level of viral receptor protein expressed at the cell surface is a critical factor for viral entry into cells. For instance, Davis et al. reported that cells expressing the highest levels of transfected DC-SIGN(R) are more susceptible to West Nile virus infection (33) than cells expressing lower levels of DC-SIGN(R). Likewise, Koutsoudakis et al. found that the entry of hepatitis C virus into cells is dependent on CD81 cell surface expression and defined a range of CD81 expression levels where viral infectivity is directly proportional to CD81 expression (34). Increasing the expression of coxsackievirus-adenovirus receptor (CAR) on poorly permissive cell lines increased the susceptibility of tumor cells to recombinant adenovirus infection (35). Human immunodeficiency virus (HIV) can utilize both CD4 and CCR5 as receptors, and the relative expression level of each receptor has been shown to influence the infectivity of different HIV isolates (36). Therefore, when measuring SARS-CoV-2 infectivity *in vitro*, it will be critical to consider the amount of ACE2 at the cell surface.

Here, we describe the stable transfection of HRT-18G cells, a human rectal cancer cell line capable of supporting betacoronavirus replication (37, 38), with plasmid vectors containing a bicistronic mRNA encoding different ACE2 orthologs and a cell surface reporter protein, mouse Thy1.1. We demonstrate that the amount of Thy1.1 is directly proportional to the amount of human ACE2 (hACE2) on the cell surface, and increasing ACE2 expression leads to both increased binding of a fluorescent RBD and increased SARS-CoV-2 pseudoviral infectivity. We also generated stable cell lines expressing either mouse ACE2 (mACE2) or domestic cat ACE2 with Thy1.1 expression equivalent to that in human ACE2-expressing cells and found that RBD binding and infectivity are absent upon the expression of mouse

ACE2, while feline ACE2 (fACE2) has an intermediate phenotype compared to human ACE2. Our system can be easily expanded to include more ACE2 orthologs to provide further insight into how RBD-ACE2 interactions impact the susceptibility or resilience of species against SARS-CoV-2 infection and transmission.

RESULTS

ACE2 binding to SARS-CoV-2 spike protein is necessary for viral infectivity. SARS-CoV-2 gains access to cells when its S-protein binds to the cell surface receptor ACE2 (1–4, 39, 40). To confirm this in our chosen cell system, we generated a cell line stably expressing human ACE2 (hACE2) to examine S-protein binding and SARS-CoV-2 pseudoviral infectivity. We generated DNA plasmids encoding a bicistronic mRNA containing human ACE2 cDNA, followed by an internal ribosome entry site (IRES) and, finally, the mouse cell surface protein Thy1.1 (Fig. 1A). The use of Thy1.1 is advantageous for several reasons. Thy1.1 is present on the cell surface and can be detected with commercially available fluorescent antibodies, allowing both the quantification of a reporter protein and the sorting of live cells stably expressing the transgene. Unlike autofluorescent reporter proteins, Thy1.1 is not inherently fluorescent and will therefore not interfere with downstream applications that depend on fluorescence detection. Because Thy1.1 and ACE2 are translated by the same mRNA, we used the relative expression of Thy1.1 to infer ACE2 expression, thus avoiding uncertainties regarding the interaction of assorted orthologs of ACE2 with available antibodies able to detect native ACE2 on the cell surface.

According to this rationale, we transfected HRT-18G cells, a human rectal cancer line capable of supporting betacoronavirus replication, with the plasmid encoding hACE2 and Thy1.1 under conditions that support stable transfection. Following transfection, cells were magnetically sorted utilizing antibodies specific for Thy1.1. Three rounds of sorting were needed to generate a stable cell line, termed HRT-18G/hACE2, with $>$95% of cells expressing Thy1.1 (Fig. 1B). In comparison to the parent cells, stably transfected cells showed significant increases in Thy1.1 and ACE2 antibody staining (Fig. 1B and C). To determine the ability of hACE2 expressed on HRT-18G cells to bind to the RBD of SARS-CoV-2 S-protein, we incubated the cells with an Alexa Fluor 647-labeled RBD protein purchased from a commercial vendor and analyzed them by flow cytometry (Fig. 1D). In contrast to the parent cells, the RBD interacted with hACE2 in a concentration-dependent manner (Fig. 1E). We also assessed the ability of hACE2 to allow viral infectivity compared to the parent cells. Both HRT-18G and HRT-18G/hACE2 cells were exposed to a vesicular stomatitis virus (VSV)-derived SARS-CoV-2 pseudovirus expressing S-protein and green fluorescent protein (GFP), termed VSV-GFP-deltaG_SARS-CoV-2 S-protein, at a multiplicity of infection (MOI) of 10 for short, defined periods of time. Cells were washed to remove excess virus and cultured for 16 h prior to the analysis of GFP expression by flow cytometry. As shown in Fig. 1F, a measurable percentage of infected HRT-18G/hACE2 cells was detected with as little as 5 min of exposure to the virus inoculum, and the number of infected cells steadily increased as the exposure time was lengthened. Finally, infected cells were visualized using fluorescence microscopy. HRT-18G and HRT-18G/hACE2 cells were infected with pseudovirus at an MOI of approximately 0.5. At 36 h postinfection, cells were examined by fluorescence microscopy for the presence of GFP-positive cells. In contrast to the parental HRT-18G cells, which showed no evidence of GFP expression, HRT-18G/hACE2 cells were readily infected with SARS-CoV-2 S-protein-expressing pseudovirus (Fig. 1G).

Taken together, these findings show that HRT-18G cells can be stably transfected and sorted based upon Thy1.1 expression to generate a cell line expressing human ACE2, which can bind SARS-CoV-2 RBD protein and support pseudoviral infection.

Cell surface ACE2 levels govern RBD binding and viral infectivity. We hypothesized that increased expression of Thy1.1 would correlate with increased ACE2 expression, leading to increased RBD binding and viral infectivity. We tested this hypothesis in two different ways. First, we transiently transfected HRT-18G cells with hACE2-IRES-Thy1.1 DNA, and 48 h later, we stained the cells for both Thy1.1 and hACE2. As shown by flow cytometry analysis (Fig. 2A), Thy1.1 staining strongly correlates with ACE2

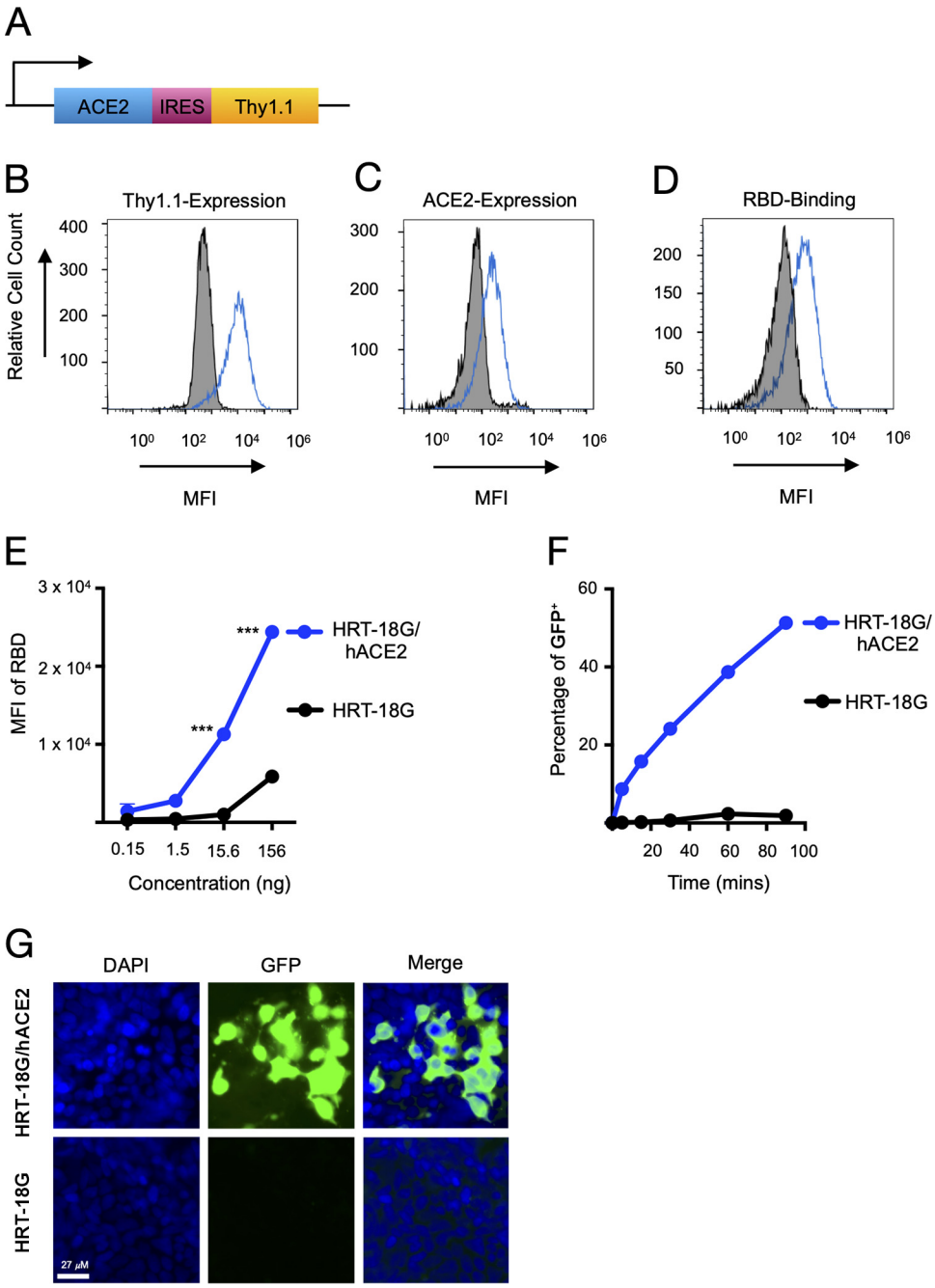

FIG 1 Recombinant SARS-CoV-2 RBD protein binds to human ACE2 and facilitates pseudoviral infectivity. (A) Schematic of the bicistronic mRNA (3,537 bp) for the production of human ACE2 (2,415 bp; 805 amino acids [aa]) and the reporter cell surface protein mouse Thy1.1 (489 bp; 163 aa). (B) HRT-18G cells were stably transfected with a plasmid containing cDNA of hACE2 and magnetically sorted for Thy1.1 expression. HRT-18G/hACE2 (blue trace) and parental HRT-18G (shaded histogram) cells were stained with fluorescent anti-Thy1.1 antibody, and expression was analyzed by flow cytometry. (C) HRT-18G cells stably expressing ACE2 (blue trace) and parent cells (shaded histogram) were incubated with fluorescent anti-ACE2 antibody and analyzed by flow cytometry. (D) HRT-18G parental cells (shaded histogram) and HRT-18G/hACE2 cells (blue trace) were incubated with the Alexa Fluor 647-labeled SARS-CoV-2 S-protein RBD and analyzed for protein binding by flow cytometry. (E) Same as panel D except that cells were incubated with a range of concentrations of the Alexa Fluor 647-labeled SARS-CoV-2 S-protein RBD and analyzed by flow cytometry. (F) HRT-18G/hACE2 and HRT-18G cells were infected with GFP-expressing SARS-CoV-2 pseudovirus at an MOI of 10 for the indicated times, washed to remove excess virus, and incubated at 37°C overnight. Infectivity was analyzed by flow cytometry 16 h later, and the percentage of GFP-positive (GFP^+) cells is reported. (G) HRT-18G/hACE2 and parent cells were infected with a GFP-expressing SARS-CoV-2 pseudovirus at an MOI of 0.5 and cultured for 36 h prior to analysis by fluorescence microscopy. Cells were stained with DAPI to delineate the nucleus. All data presented are representative of results from three independent experiments. Statistical significance is indicated (***, $P < 0.0001$). MFI, mean fluorescence intensity.

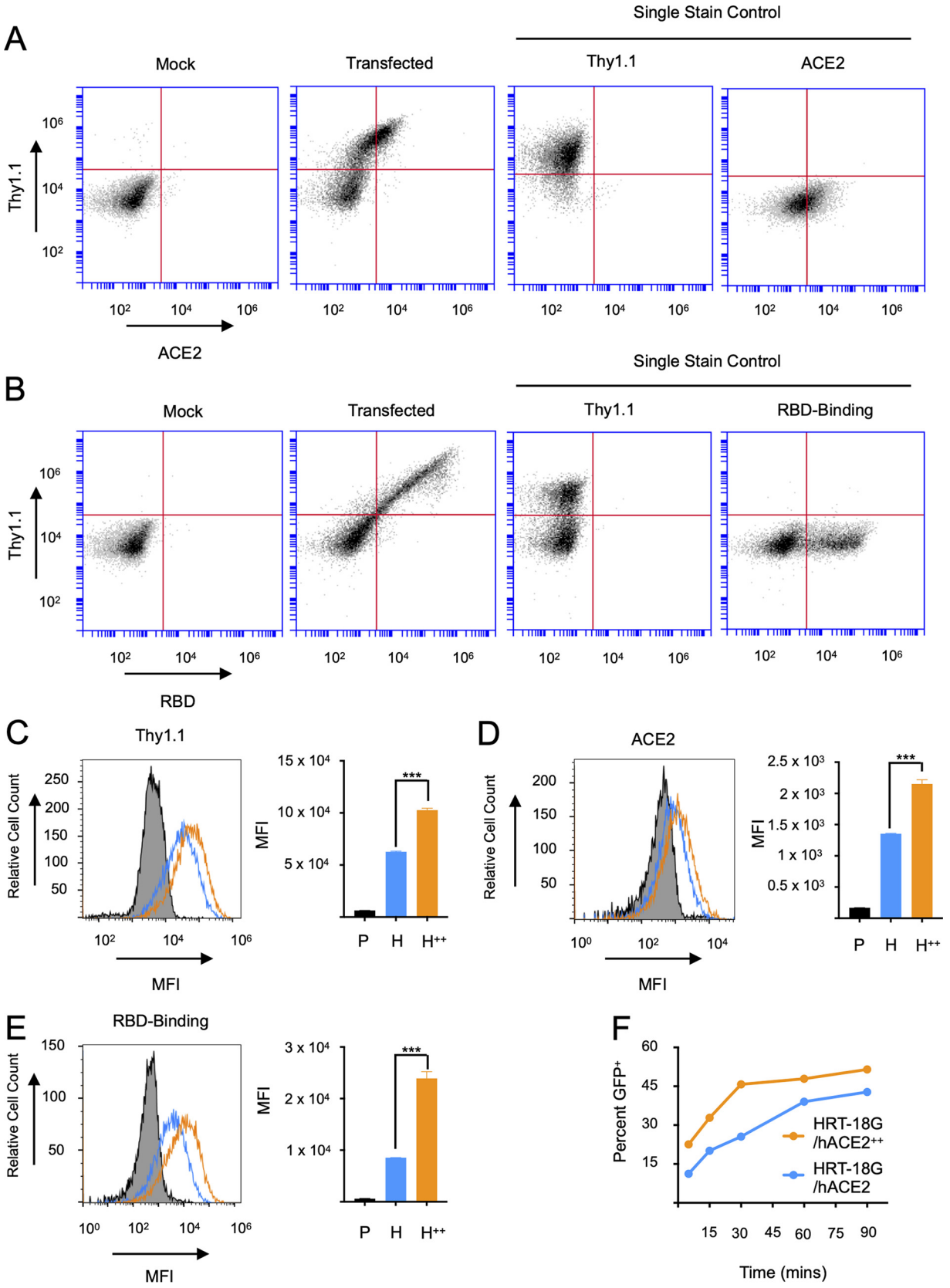

FIG 2 Increased ACE2 expression potentiates SARS-CoV-2 RBD binding and pseudoviral infectivity. (A) HRT-18G cells were transiently transfected with cDNA encoding hACE2 and Thy1.1 in a bicistronic cassette, and 2 days later, they were stained with fluorescently labeled anti-Thy1.1 and -ACE2 antibodies and analyzed by flow cytometry. Single-antibody labeling controls are also depicted. (B) Cells were stained

(Continued on next page)

levels detected by antibody staining. As a control, we show individual Thy1.1 and ACE2 staining, which resulted in no overlap in signal (Fig. 2A). To determine the interaction of transiently expressed hACE2 with the RBD of S-protein, we stained both HRT-18G and HRT-18G/hACE2 cells with Thy1.1 and the fluorescently labeled SARS-CoV-2 RBD protein. Consistent with the data shown in Fig. 1D and E, a strong positive correlation was seen between Thy1.1 expression and RBD binding (Fig. 2B), while staining with either Thy1.1 or fluorescent RBD protein individually demonstrated no overlap in signal.

Next, we fluorescently sorted HRT-18G/hACE2 cells based upon Thy1.1 staining to isolate the cells with the highest expression levels of Thy1.1, designated HRT-18G/hACE2++. As expected, the Thy1.1 expression level was significantly higher in these cells than in both the parent cells and HRT-18G/hACE2 cells (Fig. 2C). To determine if Thy1.1 expression is relative to the expression of ACE2, we stained the HRT-18G/hACE2 and HRT-18G/hACE2++ cell lines with ACE2 antibodies. Consistent with the Thy1.1 expression level, HRT-18G/hACE2++ cells showed an increase in ACE2 expression compared to the parent cells and HRT-18G/hACE2 cells (Fig. 2D). HRT-18G, HRT-18G/hACE2, and HRT-18G/hACE2++ cells were then labeled with a specific concentration of fluorescent RBD and analyzed by flow cytometry. HRT-18G/hACE2++ cells showed a distinct shift in the fluorescence intensity compared to the parental cells and a significant increase compared to HRT-18G/hACE2 cells (Fig. 2E). Finally, to confirm the importance of differential ACE2 expression for viral infectivity, we conducted a time course infection with the VSV-GFP-deltaG_SARS-CoV-2 S-protein pseudovirus. We hypothesized that cells with more ACE2 expression at the cell surface would be more susceptible when exposed to virus for brief periods of time. Consistent with the results for S-protein binding to ACE2, the percentage of infected, GFP-positive cells was higher in cells expressing high levels of ACE2 (Fig. 2F).

Together, these data indicate that measuring Thy1.1 levels in our system is a good proxy for human ACE2 levels, and alterations in the level of ACE2 at the cell surface can impact S-protein binding and viral infectivity.

ACE2 orthologs show different degrees of SARS-CoV-2 spike protein binding. Given the zoonotic nature of SARS-CoV-2 (8, 41), it is necessary to reliably predict the susceptibility of both wild and domestic animals to SARS-CoV-2 infection, which is controlled in part by the affinity of S-protein for ACE2. Our data indicate that the level of ACE2 at the cell surface can influence both the binding of the RBD of the SARS-CoV-2 S-protein as well as viral infectivity. Therefore, studies comparing different vertebrate ACE2 orthologs need to account for the relative levels of ACE2 expressed at the cell surface.

We created two additional HRT-18G cell lines expressing either domestic feline or mouse ACE2 (mACE2) orthologs using the Thy1.1 bicistronic expression system. Compared to HRT-18G/hACE2 cells, both HRT-18G/fACE2 (feline ACE2) and HRT-18G/mACE2 (mouse) cells expressed equivalent levels of Thy1.1 (Fig. 3A) and therefore likely have similar levels of ACE2 mRNA. To confirm the equivalent mRNA levels of ACE2, mRNA was extracted from cells, reverse transcribed to cDNA, and quantified by quantitative PCR (qPCR). The relative expression level of ACE2 was compared to that of glyceraldehyde-3-phosphate dehydrogenase (GAPDH). As shown in Fig. 3B, all cell lines had equivalent ACE2 mRNA levels. Cells were then stained with antibodies for human ACE2 (as used in Fig. 1 and 2), and only HRT-18G/hACE2 cells stained positive for ACE2 (Fig. 3C), indicating that this particular monoclonal antibody does not recognize either feline or mouse ACE2. To demonstrate that different

FIG 2 Legend (Continued)
with fluorescently labeled anti-Thy1.1 antibody and the Alexa Fluor 647-labeled SARS-CoV-2 S-protein RBD and analyzed by flow cytometry. Histograms of individual protein-labeled cells are also depicted. (C to E) HRT-18G/hACE2 cells (blue traces) were fluorescently sorted based on Thy1.1 expression to generate the cell line HRT-18G/hACE2++ (orange traces). HRT-18G/hACE2 (H) and HRT-18G/hACE2++ (H^{++}) cells and parental HRT-18G cells (P) (shaded histograms) were then incubated with anti-Thy1.1 (C) or anti-ACE2 (D) antibody or the Alexa Fluor 647-labeled SARS-CoV-2 S-protein RBD (E) and analyzed by flow cytometry. Histograms and quantitative MFI measurements are representative of results from three independent biological replicates. (F) HRT-18G/hACE2 and HRT-18G/hACE2++ cells were infected with GFP-expressing SARS-CoV-2 pseudovirus for the indicated times, washed to remove excess virus, incubated in complete medium for 16 h, and analyzed by flow cytometry for GFP expression. All data presented are representative of results from three independent biological experiments. Statistical significance is indicated (***, $P < 0.0001$).

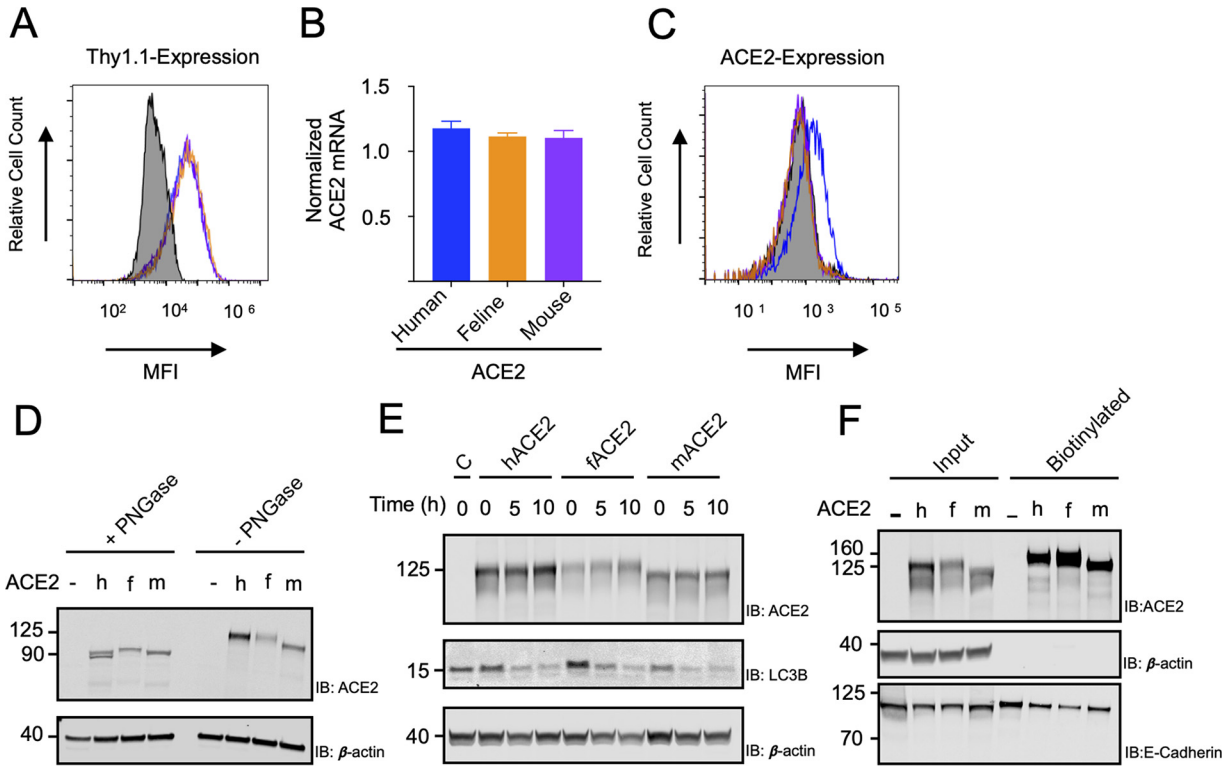

FIG 3 Human (h), feline (f), and mouse (m) ACE2 orthologs are glycosylated, metabolically stable, and detected at the cell surface in stably transfected HRT-18G cells. (A) HRT-18G cells were stably transfected with IRES-Thy1.1 plasmids containing cDNAs of human (blue), feline (orange), and mouse (purple) ACE2 and magnetically sorted until equivalent levels of the reporter protein Thy1.1 were expressed on all three cell lines. Staining of parental HRT-18G cells is shown as a negative control (shaded histogram). (B) RNA was isolated from equal numbers of HRT-18G/hACE2, HRT-18G/fACE2, and HRT-18G/mACE2 cells. cDNAs were made from extracted RNAs of the tested cell lines, and qPCR was performed using GAPDH as a housekeeping gene. C_T values from ACE2 amplifications were normalized to C_T values from GAPDH, and the average fold changes from three independent experiments are shown. (C) To confirm the specificity of the ACE2 antibody for human ACE2, HRT-18G/hACE2 (blue), HRT-18G/fACE2 (orange), HRT-18G/mACE2 (purple), and HRT-18G (shaded histogram) cells were simultaneously incubated with fluorescently labeled ACE2 antibody and analyzed by flow cytometry. (D) HRT-18G cells expressing the indicated ACE2 orthologs were lysed and either mock treated or deglycosylated by incubation with PNGase F. Cell lysates were then resolved by SDS-PAGE and immunoblotted (IB) with polyclonal antibodies to ACE2 or β-actin. Molecular weight markers are indicated. (E) Cells were cultured with CHX for 0, 5, or 10 h, followed by lysis, SDS-PAGE, and Western blot analysis for either ACE2, β-actin, or LC3B. C, control: HRT-18G cells which do not express any ACE2 ortholog. (F) Cell surface proteins were biotinylated prior to cell lysis. Biotin-conjugated proteins were isolated using a streptavidin agarose slurry and analyzed by Western blotting for ACE2, E-cadherin, and β-actin.

ACE2 orthologs were expressed by each cell line, we examined total cell lysates with a commercially available polyclonal antibody raised against a recombinant human ACE2 protein. Western blot analysis demonstrates that ACE2 is detectable in all three cell lines and absent from the parent cell line (Fig. 3D). Treatment of cell lysates with peptide-*N*-glycosidase F (PNGase F) resulted in a shift in the apparent molecular weight of ACE2 (Fig. 3D), demonstrating that each ACE2 ortholog is glycosylated.

It is possible that different orthologs of ACE2 are metabolically unstable in human cells. To test this, we treated cells with cycloheximide (CHX) to prevent new protein synthesis and measured the levels of each ACE2 ortholog over time by Western blotting. As shown in Fig. 3E, each ACE2 ortholog is highly stable when expressed by HRT-18G cells, as no appreciable ACE2 degradation is observed, even 10 h after blocking protein synthesis. As a control, we measured the levels of LC3B, a rapidly degraded protein involved in autophagy (42). As expected, the levels of LC3B were reduced following CHX treatment (Fig. 3E).

We next examined ACE2 ortholog localization to the cell surface. Cell surface proteins were selectively biotinylated and isolated by binding to streptavidin. All ACE2 orthologs were detected in the cell surface fraction (Fig. 3F). Cytosolic β-actin was absent from the cell surface fraction, whereas the cell surface marker E-cadherin was present at the cell surface of all tested cell lines (Fig. 3F), demonstrating the surface

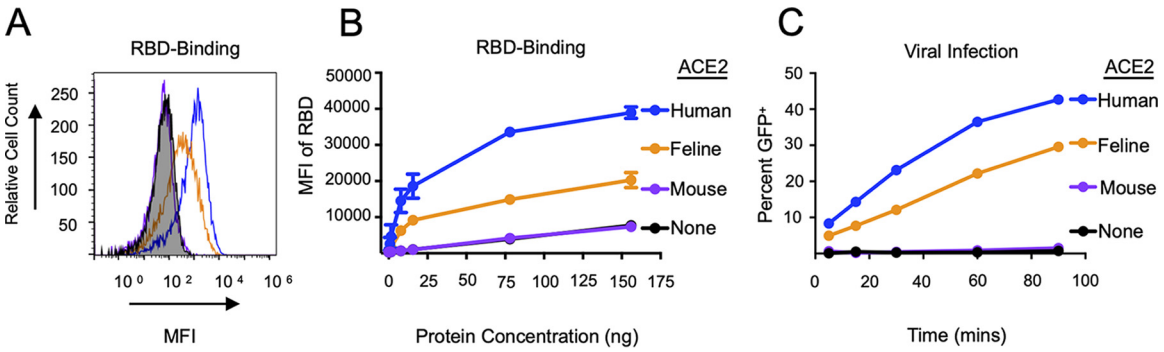

FIG 4 SARS-CoV-2 RBD binding and viral infectivity with different ACE2 orthologs. (A) HRT-18G (shaded histogram), HRT-18G/hACE2 (blue trace), HRT-18G/fACE2 (orange trace), and HRT-18G/mACE2 (purple trace) cell lines were incubated with 7.8 ng of the Alexa Fluor 647-labeled SARS-CoV-2 S-protein RBD and analyzed for SARS-CoV-2 S-protein RBD/ACE2 binding by flow cytometry. (B) Same as panel A except that cells were incubated with different concentrations of the Alexa Fluor 647-labeled RBD. The MFI of the population is reported on the *y* axis. (C) HRT-18G/hACE2, HRT-18G/fACE2, HRT-18G/mACE2, and HRT-18G cells were infected with GFP-expressing SARS-CoV-2 pseudovirus for the specified times, washed to remove excess virus, and incubated for 16 h, and GFP-expressing cells were quantified by flow cytometry. All data presented are representative of results from three independent biological experiments.

specificity of biotinylation. Therefore, human, mouse, and feline ACE2 orthologs expressed in HRT-18G cells are metabolically stable, glycosylated, and localized at the cell surface. Given that the levels of Thy1.1 and ACE2 mRNAs are nearly identical in these cells, these data suggest that ACE2 ortholog expression levels will be similar between cell lines.

We then tested SARS-CoV-2 RBD interactions with each cell line by incubating fluorescently labeled RBD protein with cells and measuring fluorescent protein binding by flow cytometry. S-protein RBD binding varied depending on the ACE2 ortholog expressed (Fig. 4A). No interaction between mouse ACE2 and S-protein was detected, as the RBD-binding pattern was the same as that in the parental HRT-18G cells (Fig. 4A and B). Human ACE2 had the highest affinity for the S-protein RBD, while feline ACE2 fell between the mouse and human orthologs (Fig. 4A and B). To further confirm the hierarchy of the S-protein RBD affinity for ACE2, we infected the same set of cell lines with SARS-CoV-2 pseudovirions and measured the number of infected cells expressing GFP. Consistent with the S-protein RBD binding with ACE2 and compared to the parent cells, HRT-18G/hACE2 cells had the largest number of infected cells, and HRT-18G/mACE2 cells had the smallest number of infected cells, while HRT-18G/fACE2 cells ranked in between the human and mouse cell lines (Fig. 4C).

DISCUSSION

SARS-CoV-2, like SARS-CoV-1, uses host ACE2 as the receptor for viral entry into cells. As such, experiments examining viral binding and entry into cells will likely be influenced by the levels of ACE2 expressed at the cell surface. As the levels of ACE2 increase on the surface of cells, there is increased binding of recombinant viral spike RBD protein to cells as well as increased viral infectivity (Fig. 2). It is therefore important when comparing the abilities of different ACE2 orthologs to interact with SARS-CoV-2 to consider the relative expression of the ACE2 ortholog being examined.

Here, we attempt to normalize ACE2 levels using a bicistronic expression system, using Thy1.1 levels as a proxy for ACE2 ortholog expression, which cannot be detected using flow cytometry due to the absence of suitable antibodies. It should be emphasized that Thy1.1 and ACE2 will be degraded with different kinetics within the cell. Therefore, Thy1.1 levels are almost certainly not equivalent to ACE2 levels on a molecule-by-molecule basis. However, when examining stably transfected, bulk-sorted cells maintained under identical cell culture conditions, Thy1.1 metabolic stability will likely be equivalent across all cell lines when Thy1.1 is expressed at identical levels. Therefore, the levels of ACE2 ortholog mRNA should also be equivalent between cells when Thy1.1 levels are equal (Fig. 3B).

At the protein level, different ACE2 orthologs may have different stabilities in cells

owing to numerous potential factors. We therefore examined the stability and trafficking of different ACE2 orthologs. All three ACE2 orthologs examined here were relatively stable proteins, as no appreciable degradation was observed 10 h following protein synthesis inhibition (Fig. 3E). If an ACE2 ortholog was inherently unstable or even a portion of the newly synthesized ACE2 was unstable, then a decrease in protein levels would have been readily observed following protein synthesis inhibition, similar to what we observed for LC3B levels (Fig. 3E). Each ACE2 ortholog was also glycosylated and readily detectable at the cell surface using biochemical means of measuring cell surface proteins, demonstrating proper posttranslational modification and trafficking. Because each ACE2 ortholog is relatively stable, glycosylated, and located on the cell surface, and the levels of Thy1.1 are equivalent between cells, it is highly likely that ACE2 orthologs are present at equivalent or nearly equivalent levels in their respective cells.

The choice of cell line is also important to consider. We selected HRT-18G cells, which are known to support betacoronavirus replication and can therefore be used in studies with SARS-CoV-2. Endogenous (human) ACE2 was also not detected in these cells by either flow cytometry or Western blotting, and the cell line proved to be resistant to infection with the pseudovirus expressing SARS-CoV-2 spike protein. This suggests that endogenous ACE2 expression is either completely absent or at a minimal level that would not support infection. The susceptibility of engineered cells expressing human ACE2 to a GFP-expressing SARS-CoV-2 pseudovirus has the added benefit of allowing researchers to conduct infectivity experiments without the need for a biosafety level 3 (BSL-3) facility. HRT-18G cells are also easily transfectable in our hands, and importantly, stable transfectants can be generated and easily sorted. We did not assess if these cells can be genetically modified through the use of retroviral gene delivery; however, such an approach is likely to be feasible.

Stably transfected cell lines are highly desirable since they can be cultured indefinitely, which negates the need to repeatedly transfect cells for each new experiment. The necessity of these renewable cells is especially important when considering newly emerging SARS-CoV-2 variants. Many of the variants of concern have altered binding of the viral S-protein to ACE2, which is of great concern to public health (43–46). It is still unknown if newly emerged variants are more infectious to other vertebrate animals or if there is a shift in the predicted susceptibility of a species to a newly emerged variant. With the presence of stably transfected cells expressing a defined amount of ACE2 that simply need to be thawed from cryogenic storage, researchers will be able to preliminarily assess if particular variants are more or less infectious to particular animals. It should be noted, however, that there is some experiment-to-experiment variability in measuring both infectivity and recombinant RBD binding to cells, and therefore, researchers should directly compare the capacities of different variants to infect cells within experiments.

The analysis of stably transfected cells overcomes the limitations associated with acute cellular stress induced by transfection. This is especially important when using a bicistronic system where the reporter protein is decoupled from the protein of interest. However, when cellular metabolism returns to normal after stable DNA integration and cell sorting, the levels of Thy1.1 are likely to reach a steady state, and the half-life of Thy1.1 will be consistent across HRT-18G-derived cell lines. This ensures that when different cell lines have equivalent Thy1.1 expression levels, they also have proportionally equivalent levels of ACE2 mRNA (Fig. 3B). As we show in Fig. 2, the levels of Thy1.1 are proportional to the ACE2 levels, which in turn correlate with both SARS-CoV-2 S-protein RBD binding and S-protein-mediated viral infectivity. In systems with transient expression of ACE2 genes (6, 27, 30, 47), the levels of ACE2 vary not only within a given population of cells but also between individual experiments. For example, as shown in Fig. 2, the transient expression of hACE2 reveals a broad level of ACE2 expression, which directly impacts S-protein RBD binding. Selecting cells based upon defined levels of Thy1.1 expression in stably transfected cells ensures consistent levels of ACE2.

This is important when comparing the interactions of S-protein with different ACE2 orthologs or homologs.

Several studies to date have expressed different ACE2 orthologs on cells to measure the potential for SARS-CoV-2 infectivity. The results have shown some consistent patterns, such as the inability of *Mus musculus* ACE2 to interact with SARS-CoV-2 (2, 24, 26, 32) (with the exception of mouse cells from the cornea [48]) or the relatively high infectivity afforded by pangolin ACE2 (6, 26, 28, 29). Results from other orthologs are more inconsistent. Conceicao et al. noted discrepancies in studies examining a variety of bat ACE2 orthologs expressed by nonpermissive cells (28). In some reports, horseshoe bat ACE2 expression leads to robust viral infectivity or S-protein binding (2, 4, 26), whereas other reports suggest more modest or very weak binding and infectivity (11, 27–31). Similar discrepancies appeared when examining palm civet ACE2, with some reports indicating poor infectivity and/or S-protein binding (11, 28–32), in contrast to other reports (2, 26). Variations in cell surface ACE2 levels between the cells used to make these comparisons likely explain some of these discrepancies. The Thy1.1 reporter system that we describe may be useful in resolving these findings.

Another advantage of our system is that it allows researchers to infer cell surface levels of ACE2 without the need for species-specific reagents. As shown in Fig. 3, a monoclonal antibody that recognizes human ACE2 fails to stain cells expressing either feline or mouse ACE2, demonstrating that commercially available reagents may not be useful for measuring the cell surface levels of different ACE2 orthologs. We and others have therefore used polyclonal antibodies to detect different ACE2 orthologs (6); however, it is not possible to determine precise levels of ACE2 with polyclonal sera, as the mixture of different antibodies with different affinities for different ACE2 orthologs confounds the ability to quantify expression. These reagents are useful in determining if ACE2 is expressed but cannot reliably determine the relative amounts of different ACE2 orthologs. The use of a reporter in a bicistronic vector that can easily be measured and used for fluorescence-based cell sorting allows us to compare SARS-CoV-2 S-protein interactions and viral infectivity without the need to develop and characterize specific reagents for each ACE2 ortholog to be studied.

The use of a bicistronic vector, while imperfect, is a robust approach to normalizing ACE2 levels between cells. Alternative methods have their own benefits and drawbacks. The expression of epitope-tagged ACE2 orthologs would allow the direct measurement of ACE2 orthologs without the need to uncouple ACE2 expression from a second protein. However, the presence of an epitope tag may induce alterations of both ACE2 structure and function, which would need to be carefully determined. While amino acid variations exist in ACE2 orthologs, which likely impact interactions with S protein, ACE2 is, overall, a highly conserved protein. The length of the extracellular ACE2 domain appears well conserved, suggesting that the insertion of an epitope tag in the extracellular domain may not be well tolerated and could alter ACE2 function, including its efficiency in mediating SARS-CoV-2 entry. Modifications to the intracellular C terminus of the ACE2 protein may be better tolerated; however, this would make the sorting of cells using antibody labeling impossible, as cells would need to be fixed and permeabilized for epitope-specific antibodies to reach the target. The addition of an autofluorescent protein fused to the C terminus could alleviate this problem; however, cells would then express high levels of fluorescent protein, which could eliminate downstream fluorescence-based experiments.

Measuring ACE2 interactions with SARS-CoV-2 may not be a perfect method for predicting species susceptibility to infection, progression to disease, and even viral transmission. For instance, both *in silico* and *in vitro* studies have suggested that ferret ACE2 and mink ACE2 interact poorly with S-protein (6, 9, 49); however, these animals are readily infected with SARS-CoV-2, often dramatically so (50–53). As the field progresses, it will behoove us to think not only of ACE2 but also of other physiological differences between species that may impact SARS-CoV-2 susceptibility.

MATERIALS AND METHODS

Cell lines, antibodies, and reagents. HRT-18G and BHK-21 cells were obtained from the American Type Culture Collection (ATCC) (Manassas, VA) and authenticated by the provider. Cell cultures were

maintained in Dulbecco's modified Eagle's medium (DMEM; Gibco, MA, USA) supplemented with 1% GlutaMAX (Gibco) and 7.5% fetal bovine serum (Atlanta Biologicals Inc., GA, USA) at 37°C in a humidified incubator containing 6% CO_2. Cell lines were checked regularly for any mycoplasma contamination and tested negative for the presence of mycoplasma contamination using a Universal mycoplasma detection kit (ATCC 30-1012K). Cell lines and their derivative cell lines were expanded and frozen in a liquid nitrogen tank in cryogenic storage at a low passage number. All Thy1.1 antibodies (unlabeled and fluorescein isothiocyanate [FITC] conjugated) were obtained from eBioscience, and allophycocyanin (APC)-coupled anti-ACE2 antibody was obtained from Abeomics. The following primary antibodies were used for Western blot analysis: mouse monoclonal β-actin (clone AC-15; Sigma), rabbit polyclonal ACE2 (catalog number 21115-1-AP; Thermo Fisher), mouse monoclonal E-cadherin (clone 4A2C7; Life Technologies), and rabbit polyclonal LC3B (clone D11; Cell Signaling). Donkey anti-mouse and anti-rabbit secondary antibodies, coupled to infrared (IR) dyes 680 and 800, respectively, were obtained from Li-Cor. All antibodies were used according to the manufacturers' protocols. An Alexa Fluor 647 protein labeling kit was obtained from Invitrogen.

Plasmid generation for ACE2 expression. All primers were obtained from Integrated DNA Technologies (IDT), and PCR products were amplified using a Veriti thermocycler (Applied Biosystems). For the generation of ACE2-expressing BHK-21 cells, human ACE2 cDNA (kindly provided by Sonja Best, NIH/NIAID) was used as a PCR template. The open reading frame of hACE2 was amplified by PCR using primers hACE2_F (5′-TGGCCTGACAGGCCCTAAAAGGAGGTCTGAACATCATC-3′) and hACE2_R (5′-TGGCCTCTGAGGCCACCATGTCA AGCTCTTCCTGGC-3′) and cloned into the pSBbi-BH vector using the SfiI restriction site. The pSBbi-BH plasmid was a kind gift from Eric Kowarz (catalog number 60515; Addgene). ACE2 orthologs were cloned into the plasmid pCAGGS-IRES-Thy1.1, as described previously (54). ACE2 cDNA sequences encoding human, feline, and murine ACE2 were ordered as gene blocks (IDT) using the NCBI reference sequences under accession numbers NM_001371415.1, NM_001039456.1, and NM_001130513.1, respectively. Gene blocks were appended with either an NheI or a ClaI site at the 5′ end and an AgeI site at the 3′ end. Gene block fragments and pCAGGS-IRES-Thy1.1 were digested with the appropriate restriction enzymes, gel purified, ligated using a Mighty Mix ligation kit (TaKaRa), cloned into competent *Escherichia coli* DH5α cells, and selected for ampicillin resistance. ACE2 sequences in positive clones were confirmed by Sanger DNA sequencing at the Oregon State University Center for Quantitative Life Sciences (CQLS). Plasmids were purified using a Qiagen HiSpeed Midi plasmid purification kit according to the manufacturer's instructions.

Cell transfection and stable cell line generation. For the generation of BHK-21 cells stably expressing human ACE2, the pCMV(CAT)T7-SB100 plasmid (encoding a transposase required to generate stable transgene-expressing cell lines) was cotransfected with pSBbi-BH hACE2 using TransIT-LT1 transfection reagent (Mirus Bio). pCMV(CAT)T7-SB100 was a kind gift from Zsuzsanna Izsvak (catalog number 34879; Addgene). The cells were selected with 250 mg/mL hygromycin B gold (InvivoGen) for 2 weeks. The surface expression of hACE2 was confirmed by flow cytometry using anti-hACE2 antibody. For HRT-18G cell lines, 2.2 μg of pCAGGS-IRES-Thy1.1 vectors encoding ACE2 orthologs was linearized with PvuI and subsequently purified, and 10^6 cells were transfected into cells using an Amaxa 96-well Nucleofector SF kit (Lonza, Basel, Switzerland) on program DS-138. Transfected cells were kept at 37°C until optimal confluence was obtained. Cells were then prepared for magnetic bead sorting using the MidiMACS separator according to the manufacturer's instructions. Briefly, cells were harvested, washed in specific sorting buffer, and incubated with anti-Thy1.1 antibody for 30 min at 4°C. Cells were washed again and incubated with anti-mouse IgG microbeads (Miltenyi Biotec, Bergisch Gladbach, Germany) for 15 min at 4°C. Washed cells were passed through an LS column, and eluted cells were mixed with fresh medium and kept at 37°C. The process was repeated until a population with >95% Thy1.1 expression was acquired.

RBD labeling. Recombinant SARS-CoV-2 spike RBD (derived from strain Wuhan-Hu-1) protein was purchased from ABclonal Technology and labeled with Alexa Fluor 674-reactive fluorescence dye according to the manufacturer's protocols (Invitrogen). HRT-18G cells and their derivatives were labeled by incubating the cells with a specific concentration of the labeled RBD for 30 min at 4°C. Cells were then washed with Hanks' balanced salt solution (HBSS) supplemented with 0.1% bovine serum albumin (BSA), resuspended in 0.1% BSA–HBSS, and analyzed with an Accuri C6 benchtop flow cytometer (BD Biosciences, San Jose, CA, USA).

Flow cytometry. HRT-18G cells stably or transiently expressing ACE2 orthologs were harvested and washed with HBSS supplemented with 0.1% BSA. Cells were then labeled with FITC-coupled anti-Thy1.1, APC-coupled anti-ACE2, or the isotype control and incubated for 30 min at 4°C. Cells were resuspended in 0.1% BSA–HBSS and analyzed using an Accuri C6 benchtop flow cytometer (BD Biosciences, San Jose, CA, USA). For GFP analysis of virally infected cells, cells were harvested, washed in phosphate-buffered saline (PBS), fixed in 2% paraformaldehyde for 15 min at room temperature, washed in excess PBS, and analyzed for GFP expression.

Virus generation, propagation, and infection. The generation of VSV-eGFP-deltaG_SARS-CoV-2 S-protein (SARS-CoV-2 pseudovirus here) was performed as follows. The SARS-CoV-2 spike full-length sequence was amplified from vector NR-52310 (BEI Resources) using primers TGTTTCCTTGACACTATGTT CGTGTTTCTGGTGCTG and CACAAGTTGATTTGGTCAGGTGTAGTGCAGTTTCAC. The backbone vector pVSV-eGFP-dG (catalog number 31842; Addgene) was linearized by PCR with primers AGTGTCAAGGAAA CAGATCGATCTC and CCAAATCAACTTGTGATATCATGC. The SARS-CoV-2 spike sequence was cloned into linearized pVSV-eGFP-dG using the In-Fusion cloning system (TaKaRa Bio Inc.). The resulting pVSV-eGFP-deltaG_SARS-CoV-2 spike vector was verified by Sanger sequencing. VSV-eGFP-deltaG_SARS-CoV-2 spike was recovered as previously described (55). Briefly, BHK-21 and 293FT cells were plated together in 6-well plates and infected with recombinant T7-expressing vaccinia virus (vTF7-3). The virus inoculum was removed after 1 h, and cells were transfected with a mixture of plasmids using TransIT-LT1 (catalog number MIR 2300; Mirus Bio), including pVSV-eGFP-deltaG_SARS-CoV-2 spike (5 μg) and N (catalog number 64087; Addgene), P (catalog number 64088; Addgene), and L (catalog number 64085; Addgene) recovery support plasmids (3, 5, and 1 μg, respectively). Forty-eight hours after transfection, the supernatant

was collected, filtered through a 0.22-μm filter to remove vTF7-3, and used to infect fresh BHK-21/hACE2-BFP cells in 6-well plates. The recovered virus was identified by fluorescence microscopy screening, passaged one more time in BHK-21/hACE2-BFP cells, and then amplified by infecting BHK-21/hACE2-BFP cells in 75-cm^2 flasks. At 72 h postinfection, the supernatant was collected, clarified of cell debris, aliquoted, and frozen at −80°C. The presence of SARS-CoV-2 spike was confirmed by Western blotting with anti-SARS-CoV-2 S1 (catalog number 40150-D004; Sino Biological) and anti-SARS-CoV-2 S2 (catalog number PA5-112048; Thermo Fisher). The inability of the rescued virus to infect BHK-21 cells in the absence of hACE2 was assessed by fluorescence microscopy and flow cytometry. The virus was propagated by infecting BHK-21/hACE2-BFP cells grown to confluence in a T-125-cm^2 flask with a low dose of virus (equivalent to a multiplicity of infection [MOI] of approximately 0.1) diluted to 15 mL in medium containing 2% fetal calf serum (FCS) for 48 h. The flask was then subjected to three rounds of freeze-thawing to lyse cells, and the medium was centrifuged at 300 relative centrifugal force (RCF) for 15 min to pellet insoluble debris. The virus-containing supernatant was aliquoted and stored at −80°C. The titer of the virus was determined on BHK-21/hACE2-BFP cells by counting visible plaques at 72 h postinfection. For infection studies, HRT-18G cells and their derivatives were plated into 24-well plates 24 h prior to infection to achieve confluence. Medium was removed, and the virus-containing supernatant was added to the cells. For kinetic infections, virus was added at an MOI of ~10, and cells were incubated for the indicated times. The virus-containing medium was removed, and cells were washed with complete medium and then incubated for 16 h in complete medium.

Fluorescence microscopy. BHK-21/hACE2-BFP cells were infected with VSV-eGFP-deltaG_SARS-CoV-2 S protein pseudovirus at an MOI of 0.5 for 2 h, with occasional agitation. Cells were then incubated with virus-free complete medium at 37°C for 24 h. The next day, cells were stained with 4′,6-diamidino-2-phenylindole (DAPI) and analyzed by Leica DMLB fluorescence microscopy. Images were taken using a QImaging Retiga 2000R digital camera and analyzed using QCapPro6.0 software.

Western blot analysis. Cells were lysed at 10^6 cells/mL for 30 min on ice in a buffer comprised of PBS with 1.0% Triton X-100 containing an EDTA-free protease inhibitor cocktail (Pierce) and then centrifuged at maximum speed to pellet insoluble material. The clarified lysate was mixed with Bolt LDS running buffer (Thermo Fisher) with 1.0 μM dithiothreitol (DTT) and heated at 97°C for 20 min. Proteins were resolved by SDS-PAGE using 4 to 12% Bolt polyacrylamide gels (Thermo Fisher) and blotted onto nitrocellulose membranes (iBlot 2). Membranes were blocked in buffer composed of Tris-buffered saline with Tween 20 (TBS-T) containing 5% dehydrated milk for 30 to 60 min at room temperature. Membranes were then exposed to primary antibody solutions in TBS-T with 0.5% milk for 60 to 120 min. Membranes were washed with TBS-T and incubated with secondary antibody solutions in TBS-T with 0.5% milk for 60 min. After extensive washing with TBS-T and water, membranes were analyzed on an Odyssey SA imaging system. In some instances, cells were treated with CHX (10 μg/mL) for 5 or 10 h prior to cell lysis. Cell lysates were also subjected to treatment with PNGase F (New England BioLabs) for 1 h prior to denaturation with Bolt running buffer and heating of the sample. For analysis of cell surface proteins, confluent cells cultured in T-75-cm^2 flasks were labeled with biotin using a cell surface biotin labeling kit (Pierce cell surface protein and biotinylation and isolation kit; Thermo Scientific) according to the manufacturer's recommended procedures. Images were taken using an Odyssey Sa infrared imaging system and analyzed using Image Studio version 3.1.

Quantitative PCR analysis. Total RNA was isolated from ~5 × 10^6 cells using a NucleoSpin RNA kit (Macherey-Nagel) according to the manufacturer's instructions. Five micrograms of total RNA from each treatment was reverse transcribed to cDNA using the RNA-to-cDNA EcoDry premix (TaKaRa) containing poly(dT) primers. Twenty nanograms of cDNA from each sample was used to perform real-time quantitative PCR (qPCR) using Fast SYBR green master mix (Applied Biosystems) according to the manufacturer's recommendations. The following primers were used to amplify 190-bp ACE2 amplicons: 5′-ACAGAAAC CAAACATAGATGTTACTGATGCAATG-3′ and 5′-CCAAGCTGTGGGRTGGCAG-3′. As a control, the following primers were used to amplify a 141-bp GAPDH product: 5′-GGTGCTCTCTGCTCCTCC-3′ and 5′-GCCAGA GTTAAAAGCAGCCC-3′. qPCR analysis was performed on the 7500 Fast Dx real-time PCR system (Applied Biosystems). The average from three technical replicates was used to determine the relative expression of ACE2 from three biological experiments. Results were obtained by normalizing the threshold cycle (C_T) values of ACE2 amplicons and expressed as fold changes relative to the values for the GAPDH amplicon controls.

Statistical analysis. All statistical analyses were performed using GraphPad Prism software version 9.0 (GraphPad Software Inc., San Diego, CA). Multiple-group comparisons were performed by one-way analysis of variance (ANOVA), followed by Tukey's or Dunnett's multiple-comparison *post hoc* test. *P* values of <0.05 were considered statistically significant.

ACKNOWLEDGMENTS

This work was funded in part by the deLaubenfels Comparative Health Research and Education Fund of the Oregon State University Foundation and National Institutes of Health grant R01AI130059 to B.P.D.

REFERENCES

1. Lan J, Ge J, Yu J, Shan S, Zhou H, Fan S, Zhang Q, Shi X, Wang Q, Zhang L, Wang X. 2020. Structure of the SARS-CoV-2 spike receptor-binding domain bound to the ACE2 receptor. Nature 581:215–220. https://doi.org/10.1038/s41586-020-2180-5.

2. Zhou P, Yang X-L, Wang X-G, Hu B, Zhang L, Zhang W, Si H-R, Zhu Y, Li B, Huang C-L, Chen H-D, Chen J, Luo Y, Guo H, Jiang R-D, Liu M-Q, Chen Y, Shen X-R, Wang X, Zheng X-S, Zhao K, Chen Q-J, Deng F, Liu L-L, Yan B, Zhan F-X, Wang Y-Y, Xiao G-F, Shi Z-L. 2020. A pneumonia outbreak associated with a new coronavirus of probable bat origin. Nature 579:270–273. https://doi.org/10.1038/s41586-020-2012-7.
3. Wang Q, Zhang Y, Wu L, Niu S, Song C, Zhang Z, Lu G, Qiao C, Hu Y, Yuen K-Y, Wang Q, Zhou H, Yan J, Qi J. 2020. Structural and functional basis of SARS-CoV-2 entry by using human ACE2. Cell 181:894–904.e9. https://doi.org/10.1016/j.cell.2020.03.045.
4. Hoffmann M, Kleine-Weber H, Schroeder S, Krüger N, Herrler T, Erichsen S, Schiergens TS, Herrler G, Wu N-H, Nitsche A, Müller MA, Drosten C, Pöhlmann S. 2020. SARS-CoV-2 cell entry depends on ACE2 and TMPRSS2 and is blocked by a clinically proven protease inhibitor. Cell 181:271–280.e8. https://doi.org/10.1016/j.cell.2020.02.052.
5. Peng R, Wu L-A, Wang Q, Qi J, Gao GF. 2021. Cell entry by SARS-CoV-2. Trends Biochem Sci 46:848–860. https://doi.org/10.1016/j.tibs.2021.06.001.
6. Liu Y, Hu G, Wang Y, Ren W, Zhao X, Ji F, Zhu Y, Feng F, Gong M, Ju X, Zhu Y, Cai X, Lan J, Guo J, Xie M, Dong L, Zhu Z, Na J, Wu J, Lan X, Xie Y, Wang X, Yuan Z, Zhang R, Ding Q. 2021. Functional and genetic analysis of viral receptor ACE2 orthologs reveals a broad potential host range of SARS-CoV-2. Proc Natl Acad Sci U S A 118:e2025373118. https://doi.org/10.1073/pnas.2025373118.
7. Rodrigues JPGLM, Barrera-Vilarmau S, Teixeira JMC, Sorokina M, Seckel E, Kastritis PL, Levitt M. 2020. Insights on cross-species transmission of SARS-CoV-2 from structural modeling. PLoS Comput Biol 16:e1008449. https://doi.org/10.1371/journal.pcbi.1008449.
8. Banerjee A, Mossman K, Baker ML. 2021. Zooanthroponotic potential of SARS-CoV-2 and implications of reintroduction into human populations. Cell Host Microbe 29:160–164. https://doi.org/10.1016/j.chom.2021.01.004.
9. Damas J, Hughes GM, Keough KC, Painter CA, Persky NS, Corbo M, Hiller M, Koepfli K-P, Pfenning AR, Zhao H, Genereux DP, Swofford R, Pollard KS, Ryder OA, Nweeia MT, Lindblad-Toh K, Teeling EC, Karlsson EK, Lewin HA. 2020. Broad host range of SARS-CoV-2 predicted by comparative and structural analysis of ACE2 in vertebrates. Proc Natl Acad Sci U S A 117:22311–22322. https://doi.org/10.1073/pnas.2010146117.
10. Othman H, Bouslama Z, Brandenburg J-T, da Rocha J, Hamdi Y, Ghedira K, Srairi-Abid N, Hazelhurst S. 2020. Interaction of the spike protein RBD from SARS-CoV-2 with ACE2: similarity with SARS-CoV, hot-spot analysis and effect of the receptor polymorphism. Biochem Biophys Res Commun 527:702–708. https://doi.org/10.1016/j.bbrc.2020.05.028.
11. Zhao X, Chen D, Szabla R, Zheng M, Li G, Du P, Zheng S, Li X, Song C, Li R, Guo J-T, Junop M, Zeng H, Lin H. 2020. Broad and differential animal angiotensin-converting enzyme 2 receptor usage by SARS-CoV-2. J Virol 94:e00940-20. https://doi.org/10.1128/JVI.00940-20.
12. Ma C, Gong C. 2021. ACE2 models of frequently contacted animals provide clues of their SARS-CoV-2 S protein affinity and viral susceptibility. J Med Virol 93:4469–4479. https://doi.org/10.1002/jmv.26953.
13. Shi J, Wen Z, Zhong G, Yang H, Wang C, Huang B, Liu R, He X, Shuai L, Sun Z, Zhao Y, Liu P, Liang L, Cui P, Wang J, Zhang X, Guan Y, Tan W, Wu G, Chen H, Bu Z. 2020. Susceptibility of ferrets, cats, dogs, and other domesticated animals to SARS-coronavirus 2. Science 368:1016–1020. https://doi.org/10.1126/science.abb7015.
14. Huang X, Zhang C, Pearce R, Omenn GS, Zhang Y. 2020. Identifying the zoonotic origin of SARS-CoV-2 by modeling the binding affinity between the spike receptor-binding domain and host ACE2. J Proteome Res 19:4844–4856. https://doi.org/10.1021/acs.jproteome.0c00717.
15. Pach S, Nguyen TN, Trimpert J, Kunec D, Osterrieder N, Wolber G. 2021. ACE2-variants indicate potential SARS-CoV-2-susceptibility in animals: a molecular dynamics study. Mol Inform 40:e2100031. https://doi.org/10.1002/minf.202100031.
16. Guo Q, Li M, Wang C, Guo J, Jiang X, Tan J, Wu S, Wang P, Xiao T, Zhou M, Fang Z, Xiao Y, Zhu H. 2021. Predicting hosts based on early SARS-CoV-2 samples and analyzing the 2020 pandemic. Sci Rep 11:17422. https://doi.org/10.1038/s41598-021-96903-6.
17. Wardeh M, Baylis M, Blagrove MSC. 2021. Predicting mammalian hosts in which novel coronaviruses can be generated. Nat Commun 12:780. https://doi.org/10.1038/s41467-021-21034-5.
18. Sote WO, Franca EF, Hora AS, Comar M, Jr. 2022. A computational study of the interface interaction between SARS-CoV-2 RBD and ACE2 from human, cat, dog, and ferret. Transbound Emerg Dis 69:2287–2295. https://doi.org/10.1111/tbed.14234.
19. Zhai X, Sun J, Yan Z, Zhang J, Zhao J, Zhao Z, Gao Q, He W-T, Veit M, Su S. 2020. Comparison of severe acute respiratory syndrome coronavirus 2 spike protein binding to ACE2 receptors from human, pets, farm animals, and putative intermediate hosts. J Virol 94:e00831-20. https://doi.org/10.1128/JVI.00831-20.
20. Guo S, Yang J, Lei Y, Liu B, Zhang W, Zhang L, Zuo Z. 2021. Which species does the virus like most: binding modes study between SARS-CoV-2 S protein and ACE2 receptor. J Mol Graph Model 105:107893. https://doi.org/10.1016/j.jmgm.2021.107893.
21. Bouricha EM, Hakmi M, Akachar J, Belyamani L, Ibrahimi A. 2020. In silico analysis of ACE2 orthologues to predict animal host range with high susceptibility to SARS-CoV-2. 3 Biotech 10:483. https://doi.org/10.1007/s13205-020-02471-3.
22. Fang S, Zheng R, Lei C, Wang J, Zheng R, Li M. 2021. Key residues influencing binding affinities of 2019-nCoV with ACE2 in different species. Brief Bioinform 22:963–975. https://doi.org/10.1093/bib/bbaa329.
23. Rendon-Marin S, Martinez-Gutierrez M, Whittaker GR, Jaimes JA, Ruiz-Saenz J. 2021. SARS CoV-2 spike protein in silico interaction with ACE2 receptors from wild and domestic species. Front Genet 12:571707. https://doi.org/10.3389/fgene.2021.571707.
24. Piplani S, Singh PK, Winkler DA, Petrovsky N. 2021. In silico comparison of SARS-CoV-2 spike protein-ACE2 binding affinities across species and implications for virus origin. Sci Rep 11:13063. https://doi.org/10.1038/s41598-021-92388-5.
25. Kumar A, Pandey SN, Pareek V, Narayan RK, Faiq MA, Kumari C. 2021. Predicting susceptibility for SARS-CoV-2 infection in domestic and wildlife animals using ACE2 protein sequence homology. Zoo Biol 40:79–85. https://doi.org/10.1002/zoo.21576.
26. Wang Q, Qiu Y, Li J, Liao C, Zhou Z, Ge X. 2021. Receptor utilization of angiotensin-converting enzyme 2 (ACE2) indicates a narrower host range of SARS-CoV-2 than that of SARS-CoV. Transbound Emerg Dis 68:1046–1053. https://doi.org/10.1111/tbed.13792.
27. Zhang H-L, Li Y-M, Sun J, Zhang Y-Y, Wang T-Y, Sun M-X, Wang M-H, Yang Y-L, Hu X-L, Tang Y-D, Zhao J, Cai X. 2021. Evaluating angiotensin-converting enzyme 2-mediated SARS-CoV-2 entry across species. J Biol Chem 296:100435. https://doi.org/10.1016/j.jbc.2021.100435.
28. Conceicao C, Thakur N, Human S, Kelly JT, Logan L, Bialy D, Bhat S, Stevenson-Leggett P, Zagrajek AK, Hollinghurst P, Varga M, Tsirigoti C, Tully M, Chiu C, Moffat K, Silesian AP, Hammond JA, Maier HJ, Bickerton E, Shelton H, Dietrich I, Graham SC, Bailey D. 2020. The SARS-CoV-2 spike protein has a broad tropism for mammalian ACE2 proteins. PLoS Biol 18:e3001016. https://doi.org/10.1371/journal.pbio.3001016.
29. Niu S, Wang J, Bai B, Wu L, Zheng A, Chen Q, Du P, Han P, Zhang Y, Jia Y, Qiao C, Qi J, Tian W-X, Wang H-W, Wang Q, Gao GF. 2021. Molecular basis of cross-species ACE2 interactions with SARS-CoV-2-like viruses of pangolin origin. EMBO J 40:e107786. https://doi.org/10.15252/embj.2021107786.
30. Li Y, Wang H, Tang X, Fang S, Ma D, Du C, Wang Y, Pan H, Yao W, Zhang R, Zou X, Zheng J, Xu L, Farzan M, Zhong G. 2020. SARS-CoV-2 and three related coronaviruses utilize multiple ACE2 orthologs and are potently blocked by an improved ACE2-Ig. J Virol 94:e01283-20. https://doi.org/10.1128/JVI.01283-20.
31. Wu L, Chen Q, Liu K, Wang J, Han P, Zhang Y, Hu Y, Meng Y, Pan X, Qiao C, Tian S, Du P, Song H, Shi W, Qi J, Wang H-W, Yan J, Gao GF, Wang Q. 2020. Broad host range of SARS-CoV-2 and the molecular basis for SARS-CoV-2 binding to cat ACE2. Cell Discov 6:68. https://doi.org/10.1038/s41421-020-00210-9.
32. Liu K, Pan X, Li L, Yu F, Zheng A, Du P, Han P, Meng Y, Zhang Y, Wu L, Chen Q, Song C, Jia Y, Niu S, Lu D, Qiao C, Chen Z, Ma D, Ma X, Tan S, Zhao X, Qi J, Gao GF, Wang Q. 2021. Binding and molecular basis of the bat coronavirus RaTG13 virus to ACE2 in humans and other species. Cell 184:3438–3451.e10. https://doi.org/10.1016/j.cell.2021.05.031.
33. Davis CW, Nguyen H-Y, Hanna SL, Sánchez MD, Doms RW, Pierson TC. 2006. West Nile virus discriminates between DC-SIGN and DC-SIGNR for cellular attachment and infection. J Virol 80:1290–1301. https://doi.org/10.1128/JVI.80.3.1290-1301.2006.
34. Koutsoudakis G, Herrmann E, Kallis S, Bartenschlager R, Pietschmann T. 2007. The level of CD81 cell surface expression is a key determinant for productive entry of hepatitis C virus into host cells. J Virol 81:588–598. https://doi.org/10.1128/JVI.01534-06.
35. Fechner H, Wang X, Wang H, Jansen A, Pauschinger M, Scherübl H, Bergelson JM, Schultheiss H-P, Poller W. 2000. Trans-complementation of vector replication versus coxsackie-adenovirus-receptor overexpression to improve transgene expression in poorly permissive cancer cells. Gene Ther 7:1954–1968. https://doi.org/10.1038/sj.gt.3301321.
36. Johnston SH, Lobritz MA, Nguyen S, Lassen K, Delair S, Posta F, Bryson YJ, Arts EJ, Chou T, Lee B. 2009. A quantitative affinity-profiling system that reveals distinct CD4/CCR5 usage patterns among human immunodeficiency

virus type 1 and simian immunodeficiency virus strains. J Virol 83:11016–11026. https://doi.org/10.1128/JVI.01242-09.
37. Jin L, Cebra CK, Baker RJ, Mattson DE, Cohen SA, Alvarado DE, Rohrmann GF. 2007. Analysis of the genome sequence of an alpaca coronavirus. Virology 365:198–203. https://doi.org/10.1016/j.virol.2007.03.035.
38. Jin L, Black W, Sawyer T. 2021. Application of environment-friendly rhamnolipids against transmission of enveloped viruses like SARS-CoV2. Viruses 13:322. https://doi.org/10.3390/v13020322.
39. Yan R, Zhang Y, Li Y, Xia L, Guo Y, Zhou Q. 2020. Structural basis for the recognition of SARS-CoV-2 by full-length human ACE2. Science 367:1444–1448. https://doi.org/10.1126/science.abb2762.
40. Walls AC, Park Y-J, Tortorici MA, Wall A, McGuire AT, Veesler D. 2020. Structure, function, and antigenicity of the SARS-CoV-2 spike glycoprotein. Cell 181:281–292.e6. https://doi.org/10.1016/j.cell.2020.02.058.
41. Salinas-Ramos VB, Mori E, Bosso L, Ancillotto L, Russo D. 2021. Zoonotic risk: one more good reason why cats should be kept away from bats. Pathogens 10:304. https://doi.org/10.3390/pathogens10030304.
42. Haspel J, Shaik RS, Ifedigbo E, Nakahira K, Dolinay T, Englert JA, Choi AMK. 2011. Characterization of macroautophagic flux in vivo using a leupeptin-based assay. Autophagy 7:629–642. https://doi.org/10.4161/auto.7.6.15100.
43. Despres HW, Mills MG, Shirley DJ, Schmidt MM, Huang M-L, Jerome KR, Greninger AL, Bruce EA. 2021. Quantitative measurement of infectious virus in SARS-CoV-2 Alpha, Delta and Epsilon variants reveals higher infectivity (viral titer:RNA ratio) in clinical samples containing the Delta and Epsilon variants. medRxiv. https://doi.org/10.1101/2021.09.07.21263229.
44. Li T, Xue W, Zheng Q, Song S, Yang C, Xiong H, Zhang S, Hong M, Zhang Y, Yu H, Zhang Y, Sun H, Huang Y, Deng T, Chi X, Li J, Wang S, Zhou L, Chen T, Wang Y, Cheng T, Zhang T, Yuan Q, Zhao Q, Zhang J, McLellan JS, Zhou ZH, Zhang Z, Li S, Gu Y, Xia N. 2021. Cross-neutralizing antibodies bind a SARS-CoV-2 cryptic site and resist circulating variants. Nat Commun 12:5652. https://doi.org/10.1038/s41467-021-25997-3.
45. Li M, Lou F, Fan H. 2021. SARS-CoV-2 variants of concern Delta: a great challenge to prevention and control of COVID-19. Signal Transduct Target Ther 6:349. https://doi.org/10.1038/s41392-021-00767-1.
46. Celik I, Yadav R, Duzgun Z, Albogami S, El-Shehawi AM, Fatimawali F, Idroes R, Tallei TE, Emran TB. 2021. Interactions of the receptor binding domain of SARS-CoV-2 variants with hACE2: insights from molecular docking analysis and molecular dynamic simulation. Biology (Basel) 10:880. https://doi.org/10.3390/biology10090880.
47. Kim Y, Gaudreault NN, Meekins DA, Perera KD, Bold D, Trujillo JD, Morozov I, McDowell CD, Chang K-O, Richt JA. 2022. Effects of spike mutations in SARS-CoV-2 variants of concern on human or animal ACE2-mediated virus entry and neutralization. Microbiol Spectr 10:e01789-21. https://doi.org/10.1128/spectrum.01789-21.
48. Ma D, Chen C-B, Jhanji V, Xu C, Yuan X-L, Liang J-J, Huang Y, Cen L-P, Ng TK. 2020. Expression of SARS-CoV-2 receptor ACE2 and TMPRSS2 in human primary conjunctival and pterygium cell lines and in mouse cornea. Eye 34:1212–1219. https://doi.org/10.1038/s41433-020-0939-4.
49. Low-Gan J, Huang R, Kelley A, Jenkins GW, McGregor D, Smider VV. 2021. Diversity of ACE2 and its interaction with SARS-CoV-2 receptor binding domain. Biochem J 478:3671–3684. https://doi.org/10.1042/BCJ20200908.
50. Berguido FJ, Burbelo PD, Bortolami A, Bonfante F, Wernike K, Hoffmann D, Balkema-Buschmann A, Beer M, Dundon WG, Lamien CE, Cattoli G. 2021. Serological detection of SARS-CoV-2 antibodies in naturally-infected mink and other experimentally-infected animals. Viruses 13:1649. https://doi.org/10.3390/v13081649.
51. Kim Y-I, Kim S-G, Kim S-M, Kim E-H, Park S-J, Yu K-M, Chang J-H, Kim EJ, Lee S, Casel MAB, Um J, Song M-S, Jeong HW, Lai VD, Kim Y, Chin BS, Park J-S, Chung K-H, Foo S-S, Poo H, Mo I-P, Lee O-J, Webby RJ, Jung JU, Choi YK. 2020. Infection and rapid transmission of SARS-CoV-2 in ferrets. Cell Host Microbe 27:704–709.e2. https://doi.org/10.1016/j.chom.2020.03.023.
52. Oreshkova N, Molenaar RJ, Vreman S, Harders F, Oude Munnink BB, Hakze-van der Honing RW, Gerhards N, Tolsma P, Bouwstra R, Sikkema RS, Tacken MGJ, de Rooij MMT, Weesendorp E, Engelsma MY, Bruschke CJM, Smit LAM, Koopmans M, van der Poel WHM, Stegeman A. 2020. SARS-CoV-2 infection in farmed minks, the Netherlands, April and May 2020. Euro Surveill 25:2001005. https://doi.org/10.2807/1560-7917.ES.2020.25.23.2001005.
53. USDA. 2020. USDA confirms SARS-CoV-2 in mink in Utah. Animal and Plant Health Inspection Service, USDA, Washington, DC.
54. Vijayasimha K, Tran MV, Leestemaker-Palmer AL, Dolan BP. 2021. Direct conjugation of NEDD8 to the N-terminus of a model protein can induce degradation. Cells 10:854. https://doi.org/10.3390/cells10040854.
55. American Association of Neurological Surgeons (AANS), American Society of Neuroradiology (ASNR), Cardiovascular and Interventional Radiology Society of Europe (CIRSE), Canadian Interventional Radiology Association (CIRA), Congress of Neurological Surgeons (CNS), European Society of Minimally Invasive Neurological Therapy (ESMINT), European Society of Neuroradiology (ESNR), European Stroke Organization (ESO), Society for Cardiovascular Angiography and Interventions (SCAI), Society of Interventional Radiology (SIR), Society of NeuroInterventional Surgery (SNIS), World Stroke Organization (WSO), Sacks D, Baxter B, Campbell BCV, Carpenter JS, Cognard C, Dippel D, Eesa M, Fischer U, Hausegger K, Hirsch JA, Shazam Hussain M, Jansen O, Jayaraman MV, Khalessi AA, Kluck BW, Lavine S, Meyers PM, Ramee S, Rüfenacht DA, Schirmer CM, Vorwerk D. 2018. Multisociety consensus quality improvement revised consensus statement for endovascular therapy of acute ischemic stroke. Int J Stroke 13:612–632.